Rheological behavior of dilute bubble suspensions in polyol

Yun Mee Lim, Dongjin Seo and Jae Ryoun Youn*

School of Materials Science and Engineering, Seoul National University, Seoul 151-742, Korea

Abstract

Low Reynolds number, dilute, and surfactant-free bubble suspensions are prepared by mechanical mixing after introducing carbon dioxide bubbles into a Newtonian liquid, polyol. The apparent shear viscosity is measured with a wide-gap parallel plate rheometer by imposing a simple shear flow of capillary numbers (Ca) of the order of $10^{-2} \sim 10^{-1}$ and for various gas volume fractions (ϕ). Effects of capillary numbers and gas volume fractions on the viscosity of polyol foam are investigated. At high capillary number, viscosity of the suspension increases as the gas volume fraction increases, while at low capillary number, the viscosity decreases as the gas volume fraction increases. An empirical constitutive equation that is similar to the Frankel and Acrivos equation is proposed by fitting experimental data. A numerical simulation for deformation of a single bubble suspended in a Newtonian fluid is conducted by using a newly developed two-dimensional numerical code using a finite volume method (FVM). Although the bubble is treated by a circular cylinder in the two dimensional analysis, numerical results are in good agreement with experimental results.

Keywords : bubble suspension, bubble deformation, foam rheology, relative viscosity, finite volume method

1. Introduction

The rheological behavior of bubble suspensions has been studied intensively because of its practical significance and complexity of the phenomena. For example, polyurethane foams have been studied for various practical applications (Park and Youn, 1992; Cho et al., 1994; Park and Youn, 995; Youn and Park, 1999; Kim and Youn, 2000; Koo et al., 2001; Lee et al., 2002). By adding gaseous bubbles into a Newtonian fluid, the bubble suspension exhibits non-Newtonian behaviors, such as elastic effects and shear- and time-dependent viscosity (Macosko, 1994). The rheological behavior of bubble suspensions can be characterized by two dimensionless parameters: the volume fraction of bubbles in suspension (ϕ) and the capillary number (Ca). The capillary number is defined as $Ca = \mu \dot{\gamma} r / \Gamma$ where μ is the viscosity of the suspending fluid, $\dot{\gamma}$ is the shear rate, r is the radius of the undeformed spherical bubble, and Γ is the surface tension.

A semi-empirical constitutive model and experimental results for bubble suspensions with gas volume fractions less than 0.5 and small bubble deformation was recently suggested by Llewellin et al. (2002). The constitutive equation proposed by their model was similar to the linear Jeffreys model. It involved viscosity of the continuous phase,

gas volume fraction, relaxation time, bubble size distribution, and empirically determined dimensionless constants. Their experiments showed the effect of volume fraction and the frequency of oscillation on the elastic and viscous components of the deformation: the viscosity of the suspension increases as the volume fraction increases at low frequency, while it decreases as the volume fraction increases at high frequency. Rust and Manga (2002) studied the relative viscosity (the ratio of the viscosity of the suspension to the viscosity of the suspending fluid) of low Reynolds number, dilute, and surfactant-free bubble suspensions in simple shear flow by using a Couette rheometer. The relative viscosity was greater than 1 at low capillary number and less than 1 at high capillary number. The suspensions showed shear thinning behavior around the capillary number of order 1.

There have been few studies reported on bubble suspensions by using a numerical method because of difficulties in numerical treatments, e.g., moving interface modeling, treatment of surface tension, and very small viscosity ratio. The viscosity ratio is defined as the ratio of viscosity between the suspended fluid and the suspending fluid. Loewenberg and Hinch (1996) conducted three-dimensional numerical simulation of a concentrated emulsion in shear flow at low Reyonlds numbers and finite capillary numbers. They used the boundary integral formulation with moving vertices along with the local fluid velocity. Their results were obtained for the volume frac-

*Corresponding author: jaeryoun@snu.ac.kr

tions up to 30% and the viscosity ratios in the range of 0 to 5. Cristini *et al.* (1998) carried out a numerical research about drop breakup in three-dimensional viscous flows by using boundary integral algorithms. Renardy and Cristini (2001) studied the effect of inertia on drop breakup under shear deformation by using a volume-of-fluid (VOF) continuous surface force algorithm. Although high Reynolds number is assumed for the numerical results on the behavior of the drop in liquid, the same density and viscosity are selected for both the drop and the liquid. So it was difficult to apply those results to bubble suspensions directly. Renardy *et al.* (2002) studied the drop deformation under shear flow at a low viscosity ratio and the effect of surfactants. The drop and the suspending fluid had equal density and viscosity ratio of 0.05. They used a VOF method to track the interfaces based on a piecewise linear reconstruction and a continuum method for modeling the interfacial tension. Anyway there are few reports on bubble suspensions for high capillary number and small viscosity ratio.

In this study the rheological behavior of dilute bubble suspensions in polyol was investigated. Various suspending fluids were prepared with different volume fractions and bubble radii, and the shear viscosity was measured with a wide-gap parallel plate rheometer. In addition to the experiment, we performed a numerical simulation of single bubble deformation between two shearing parallel plates by using a finite volume method. A two-dimensional numerical code was formulated with a multigrid algorithm, and deformed bubble shapes, pressure, and velocity fields were obtained with respect to time for high capillary number and small viscosity ratio.

2. Experiments

2.1. Preparation of bubble suspensions

The suspending fluid used in our experiment is propylene oxide based polyol that is surfactant free. Polyol shows Newtonian behavior with the viscosity of 17 Pa · s and the density of 1070 kg/m^3 at room temperature. Suspensions are prepared by mechanical mixing after carbon dioxide gas is injected into polyol. Compressed carbon dioxide gases are supplied to the polyol from the end of a hollow tube and the beater breaks the emerging gas bubbles into numerous small ones by rotating the shaft. A schematic diagram for the formation of spherical bubbles is shown in Fig. 1.

Gas volume fractions are adjustable by controlling stirring time. Increasing stirring time leads to increase in the gas volume fraction. It is difficult to achieve large volume fraction because of the lack of surfactants and the low viscosity of polyol. In this study, volume fractions of the prepared suspensions are 0.047, 0.073, 0.114, and 0.146.
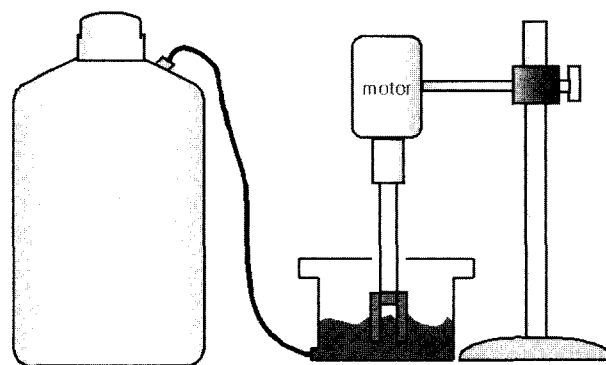

Fig. 1. Schematic diagram of the experimental set-up used for generation of bubble suspension.

2.2. Measurements of rheological properties

After suspensions are prepared, they are transferred to the BROOKFIELD DV-II+ viscometer with rotating wide-gap parallel plates and shear viscosity under the imposed shear rate is measured. All experiments are performed at $22.0 \pm 0.2°C$. In order to neglect inertia effects, the shear rates applied in our tests are 0.34, 0.69, 1.39, and 2.78 (s^{-1}) such that the maximum Reynolds number was less than 10^{-5}.

To measure the bubble size distribution, suspensions are pressed between two glass plates with 0.2 mm gap. Digital images are taken by using a polarized optical microscope with 50× magnification. A typical image contains about 120 bubbles with radii ranging from 8 to 500 μm. Average bubble radius is calculated from the radius distribution at each volume fraction.

According to the Hadamard-Rybczynski (Llewellin *et al.*, 2002), bubble rising during the experiments can be ignored if the maximum test duration is within about 3 minutes when the largest bubble radius in suspension is 500 μm.

3. Numerical modeling

In this study, we used a pressure based finite volume method for unstructured meshes that includes the SIMPLE algorithm (Patankar, 1981) for two-dimensional fluid flow problem. Cell-based, co-located storage is used for all physical variables. For treating the moving interface, an explicit high resolution scheme that is similar to the CIC-SAM method (Ubbink and Issa, 1999) is used. The bubble suspension is modeled as two phases of incompressible Newtonian fluids with different viscosities.

Computational domain is filled with two different fluids, suspending fluid and air, and has a moving interface. Assuming an isothermal incompressible Newtonian fluid, general governing equations can be written as follows:

Continuity : $\nabla \cdot v = 0$ (1)

Momentum Equation : $\rho\left(\dfrac{\partial v}{\partial t} + v \cdot \nabla v\right) = -\nabla p + \mu \nabla^2 v + f_\sigma$ (2)

where ρ is density, t is time, v is the velocity vector, p is pressure, μ is the viscosity, and f_σ is the force due to surface tension.

In order to track the interface between suspending fluid and air, the fractional volume function $f(x, t)$ is defined such that

$$f(x, t) = \begin{cases} 1 & \text{for the point } (x, t) \text{ filled with fluid} \\ 0 & \text{for the point } (x, t) \text{ filled with air} \end{cases}$$ (3)

The fractional volume function is governed by a scalar advection equation,

$$\dfrac{\partial f}{\partial t} + v \cdot \nabla f = 0$$ (4)

This equation is solved explicitly by combining the Hyper-C scheme and the ULTIMATE-QUICKEST scheme (Leonard, 1991). The interface is located within the cells whose average value of f lies between 0 and 1.

For these cells, material properties such as viscosity and density are interpolated by using the following equations.

$$\mu = \mu_m f + \mu_a(1 - f)$$ (5)

$$\rho = \rho_m f + \rho_a(1 - f)$$ (6)

where the subscript m and a represent the suspending fluid and air, respectively.

Surface tension force is formulated with the continuum surface force (CSF) concept (Brackbill *et al.*, 1993) and given by

$$f_\sigma = -(\Gamma \nabla f)\nabla \cdot \left(\dfrac{\nabla f}{|\nabla f|}\right)$$ (7)

More detailed numerical schemes are described in the previous paper (Seo *et al.*, 2003). In addition, multigrid algorithms (Yan and Thiele, 1998) are incorporated into the numerical code to increase the rate of convergence and reduce the calculation time compared with equivalent single-grid schemes.

4. Results and discussion

4.1. Experimental results

Average bubble radius of each volume fraction is calculated from radius distribution. Optical micrographs of bubbles and radius distribution at $\phi = 0.114$ are shown in Fig. 2. The suspensions are polydispersed and there is a linear relationship between the average bubble radius and the volume fraction as shown in Fig. 3. As volume fraction increases, the average bubble radius decreases due to breakage of gas bubbles into small bubbles during preparation of bubble suspension. The relationship is presented as follows:
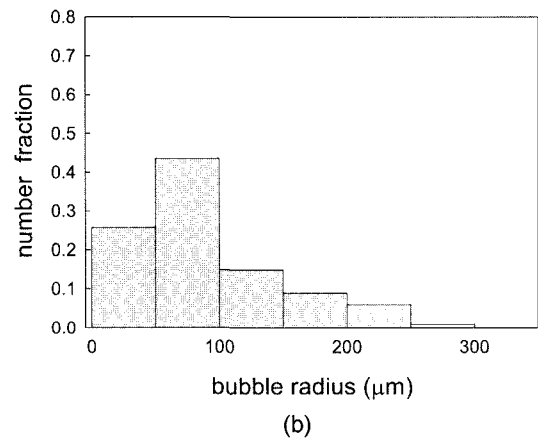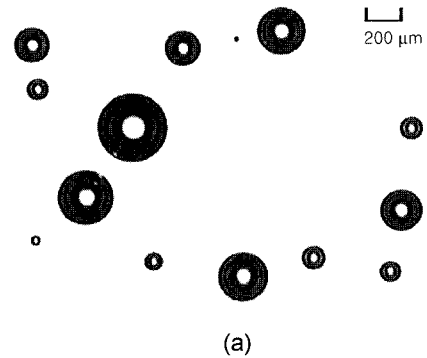

(a)

(b)

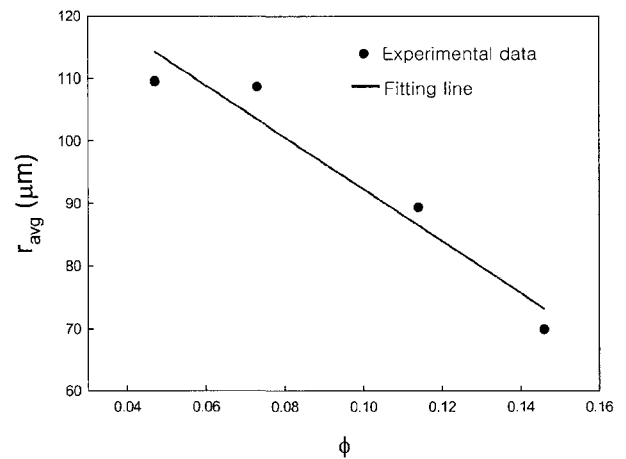**Fig. 2.** Optical micrographs of bubbles and radius distribution at $\phi = 0.114$.

Fig. 3. Relationship between average bubble radius and volume fraction.

$$r_{avg} = 133 - 414\phi \ (\mu m)$$ (8)

where r_{avg} is the average radius of the bubble.

Relative viscosity variation with respect to the capillary number at each volume fraction is shown in Fig. 4. The experiments have been carried out for small range of capillary numbers due to the difficulties in experiments. There is no breakage of bubbles under shear flow during exper-
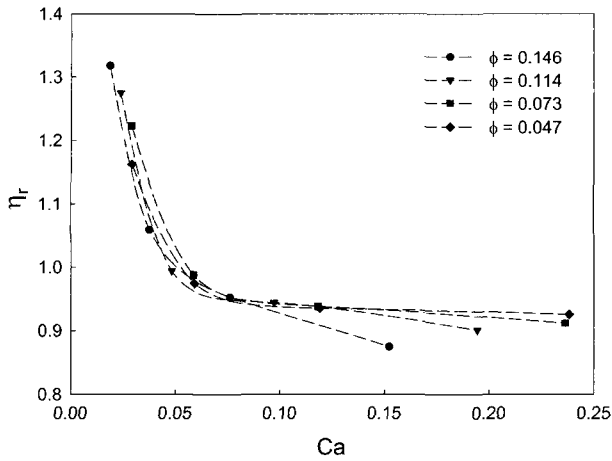
**Fig. 4.** Variation of relative viscosity with respect to different capillary numbers.

iments because the capillary number is much less than the critical capillary number (Ca_{crit}) where bubble breakup occurs. Ca_{crit} for bubble suspension is known to be greater than 1000 in a simple shear flow (Tucker and Moldenaers, 2002). Therefore the change of capillary number can be considered as that of shear rate. The suspensions show shear thinning behavior although the suspending fluid is Newtonian, which is caused by the bubble deformation in shear flow. The suspending fluid flows easier when the bubble deformation becomes larger, so the relative viscosity decreases as the shear rate increases.

It has been reported that relative viscosity at low and high capillary number has constant value. Relative viscosity is $(1 + \phi)$ at low capillary number according to the Taylor (1932) and $(1 - 5/3\phi)$ at high capillary number according to the Mackenzie (1950). But constant relative viscosity at low capillary number was not observed in this study. It may be caused by the polydispersity of the suspensions (Llewellin et al., 2002). We plotted the relative viscosity with respect to the volume fraction at two different shear rates in order to investigate the effect of volume fraction on relative viscosity. As shown in Fig. 5, increasing volume fraction leads to an increase in viscosity at low shear rates, whereas viscosity decreases as volume fraction increases at high shear rates. These results can be represented as the following equations:

$$\eta_r = 1 + \frac{3}{2}\phi \quad \text{at} \quad \dot{\gamma} = 0.34 \ \text{s}^{-1} \tag{9}$$

$$\eta_r = 1 - \frac{1}{2}\phi \quad \text{at} \quad \dot{\gamma} = 2.78 \ \text{s}^{-1} \tag{10}$$

where η_r is the relative viscosity. The difference between the measured value and the theoretical predictions by Taylor and Mackenzie is due to the hydrodynamic interaction between bubbles, polydispersity of bubbles, and the buoyant effect that causes many bubble to exist right below the upper plate of the parallel plate viscometer. At low cap-
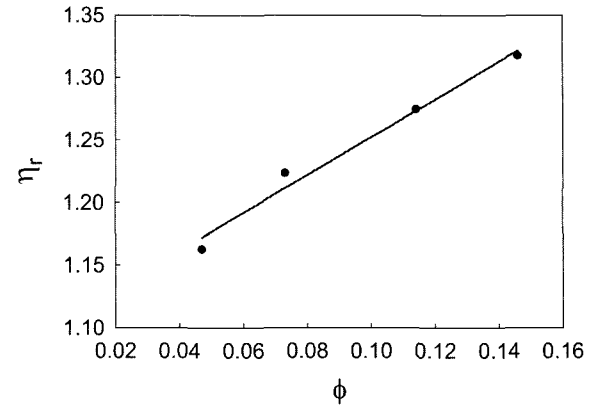
(a) $\dot{\gamma} = 0.34$ (s^{-1})
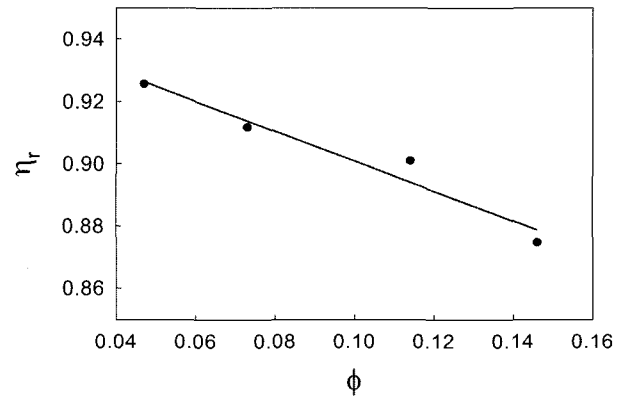
(b) $\dot{\gamma} = 2.78$ (s^{-1})

Fig. 5. Effects of the volume fraction on the relative viscosity for different shear rates.

illary number or low shear rate, restoring force by surface tension is larger than viscous force so that the shape of bubbles changes rarely and is almost maintained as a sphere. Therefore, the bubbles act as obstacles against the flow. On the other hand, bubbles deform with flow at high capillary numbers so that the negligible viscosity of air compared with that of the suspending fluid causes the viscosity of suspensions to decrease.

Frankel and Acrivos (1970) derived a general constitutive equation for dilute emulsions by considering the small deformations of a droplet in a time-dependent shearing flow. The equation can be reproduced as

$$\eta_r = \frac{1 + ((6/5)Ca)^2 + \phi(1 - (12/5)Ca^2)}{1 + ((6/5)Ca)^2} \tag{11}$$

We formulated a constitutive equation that has a similar form to the Frankel and Acrivos equation. Although there is no physical basis, this equation is useful as it matches the experimental data. The general fitting equation is expressed as the following.
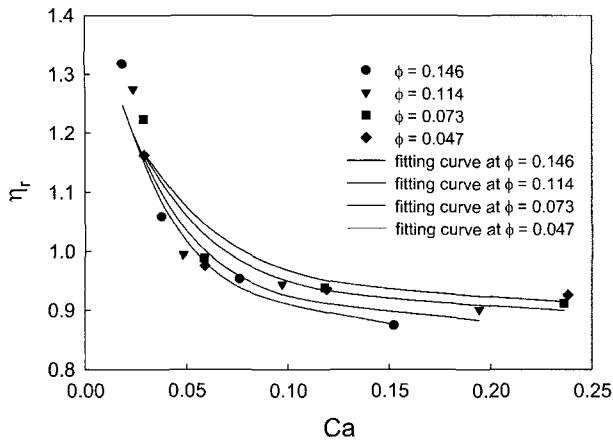
$$\eta_r = \frac{a + cCa^2}{1 + bCa^2} \tag{12}$$

Fig. 6. Fitted curves according to the general constitutive equation and experimental data.

In order to find a, b, and c as a function of ϕ, every experimental data is fitted to the Equation (12) at each volume fraction. Relationship between each parameter and the volume fraction is obtained as below.

$$a = 1.22 + \phi \tag{13}$$

$$\frac{c}{b} = 0.92 - 0.5\phi \tag{14}$$

$$b = 239 + 4123\phi \tag{15}$$

So the general constitutive equation is represented as

$$\eta_r = \frac{1.22 + \phi + (22.1 + 369\phi - 202\phi^2)\left(\frac{16}{9}Ca\right)^2}{1 + (23.9 + 412\phi)\left(\frac{16}{9}Ca\right)^2} \tag{16}$$

Fig. 6 shows the experimental data and the above general constitutive equation with respect to each volume fraction.

4.2. Numerical results

Shearing of a bubble between two parallel plates is modeled numerically as shown in Fig. 7. The upper and lower plates move in opposite direction with the same speed of $U/2$. The distance between the plates, d, is 0.5 m and the length of plates, L, is 1 m. The bubble diameter, $2r$, is 0.3 or 0.2 m and located at the center between the two plates. So the volume fraction of the bubble, ϕ, is 0.15 or 0.064. For convergence of numerical simulation, density of fluid and bubble is set to the same value of 0.1 kg/m^3, which are not realistic but will not affect the solution because the creeping flow is considered. Viscosities of the fluid and the bubble are assumed to be 10000 Pa·s and 100 Pa·s respectively, so that the viscosity ratio $\lambda = 0.01$. We tested other cases where the viscosity ratio is up to 0.001, but there was no difference in solution and it took longer time to obtain converged solutions. For the system of bubble suspension, capillary number and Reynolds number are
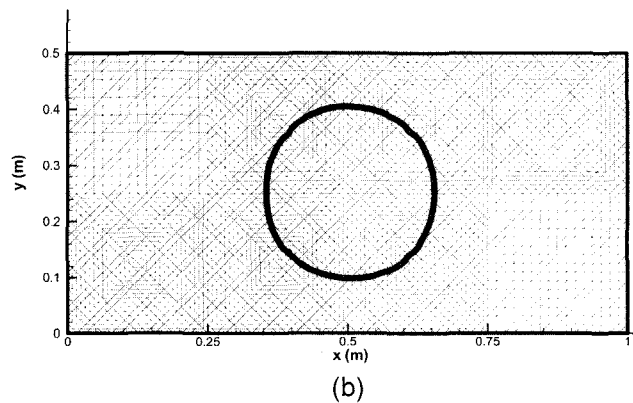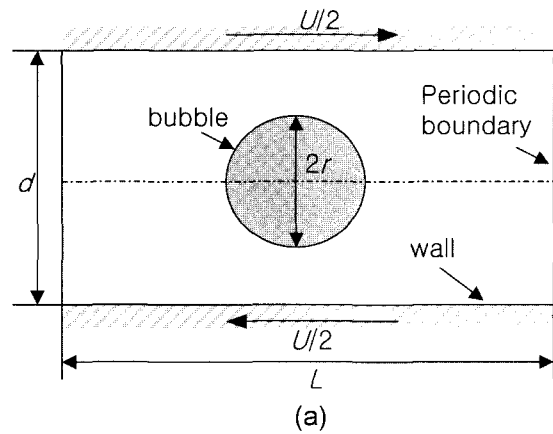

Fig. 7. Two-dimensional finite volume analysis for a single bubble suspended in a Newtonian fluid assuming simple shear flow: (a) geometry used for numerical simulation and (b) Initial bubble shape with $\phi = 0.15$ and mesh with 3861 nodes and 7168 elements.

defined as follows

$$Ca \equiv \frac{\mu_m \dot{\gamma} r}{\Gamma} = \frac{2U\mu_m r}{\Gamma d} \tag{17}$$

$$Re \equiv \frac{\rho_m \dot{\gamma} r}{\mu_m} = \frac{2U\rho_m r^2}{\mu_m d} \tag{18}$$

Here U is 0.1 m/s so that Re is small enough to assume creeping flow. Periodic boundary condition is applied to the left and right side of the computational domain. Fig. 7(b) shows the initial bubble shape with $\phi = 0.15$ and the finite volume mesh with 3861 nodes and 7168 elements. We obtained the mesh-independent solution at high capillary number, but finer mesh yielded better solution at low capillary number. Therefore we exclude the results at Ca < 0.1 because it took too long to run our code in the Pentium III PC.

When the surface tension is large (low Ca), it is difficult to achieve convergence and obtain physically meaningful solutions due to the mesh dependence of the solution. In the case of large surface tension, small wiggles in the surface result in large changes in the solutions. Shapes of the deformed bubble with $\phi = 0.15$ in 8 seconds are shown in
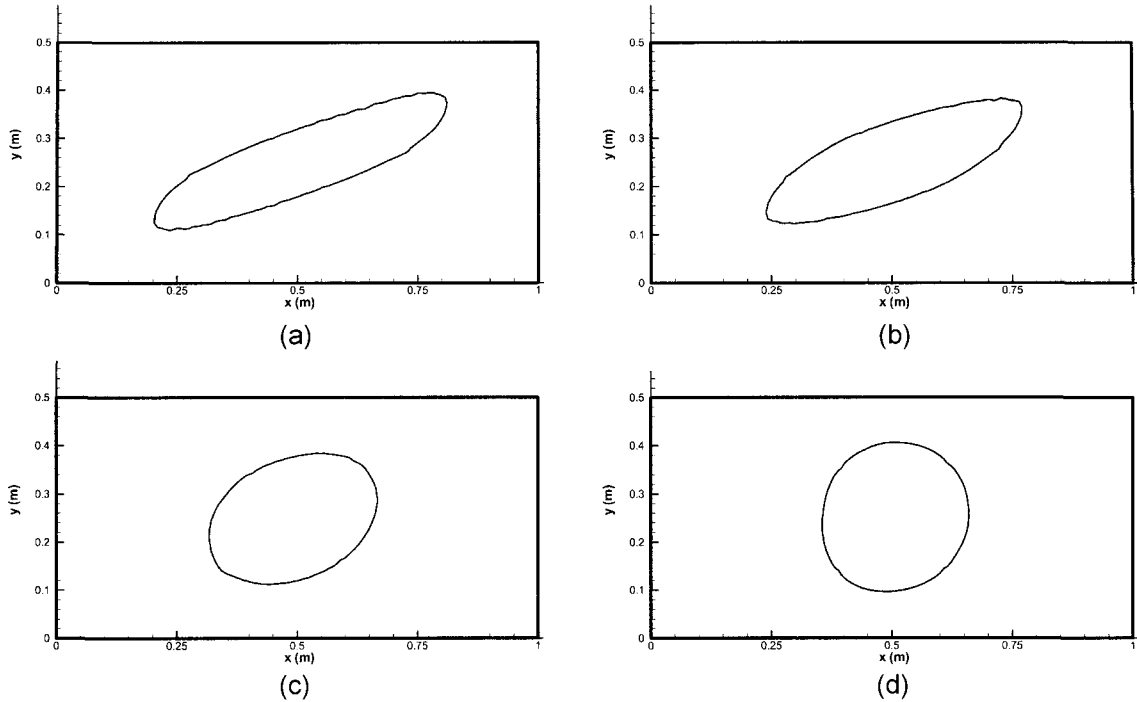
Fig. 8. Shape of the deformed bubble with $\phi = 0.15$ at $t = 8$ s; (a) $Ca = 10$, (b) $Ca = 1$, (c) $Ca = 0.1$, and (d) $Ca = 0.01$.
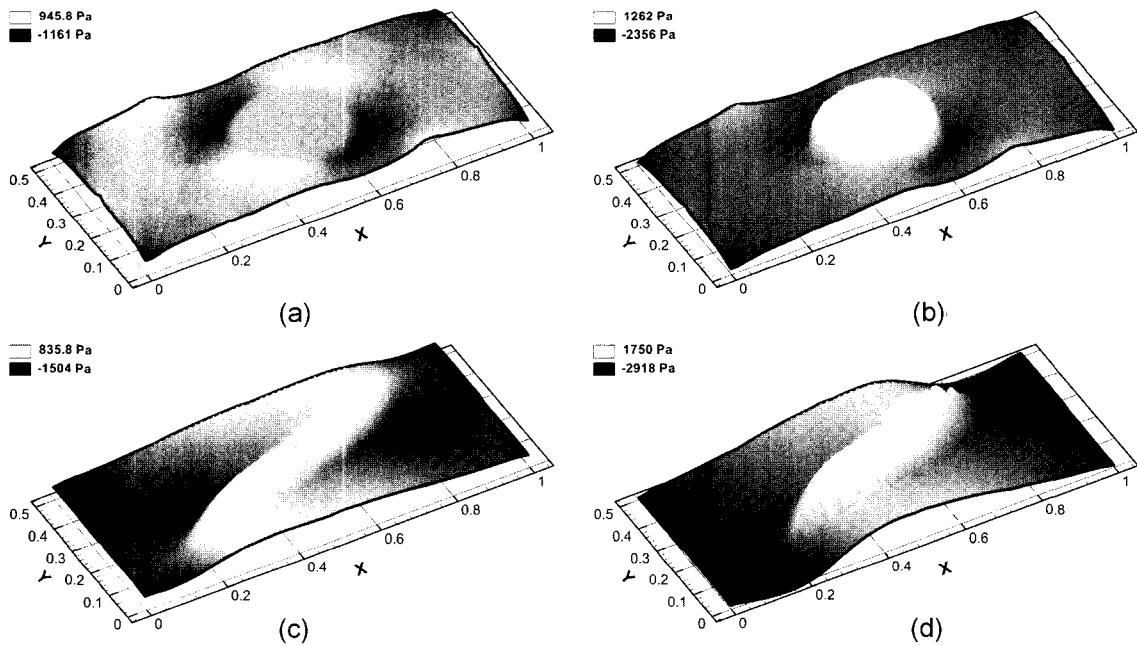

Fig. 9. Pressure field when volume fraction of gas is 0.15 (a) $Ca = 10$, $t = 0.01$ s (b) $Ca = 1$, $t = 0.01$ s (c) $Ca = 10$, $t = 8$ s (d) $Ca = 1$, $t = 8$ s.

Fig. 8 for different capillary numbers. As surface tension increases, the bubble resists deforming from its original spherical shape. In the case of $Ca = 0.01$, the bubble shape is almost the same as the sphere. Fig. 9 represents the pressure fields of the entire domain at two different times and capillary numbers when the bubble with the volume frac-

tion of 0.15 is sheared. The pressure is represented as the gray contour plot. Due to surface tension, pressure inside of the bubble is higher than suspending fluid. The assumption that the air bubble is incompressible is acceptable because the average pressure around the bubble changes so little that the volume change of the air bubble is negligible
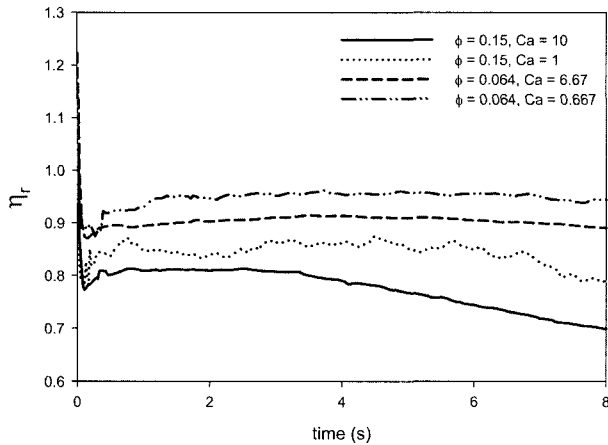
Fig. 10. Transient variation of the relative viscosity for different capillary number assuming simple shear flow.

Fig. 11. Effects of capillary number on the relative viscosity when the bubble is slightly deformed.

during the simple shear flow. Right after the bubble begins to deform, pressure is low in the upwind region of the bubble because viscosity decreases drastically across the interface between air and suspending fluid. On the other hand, pressure is high in the downwind region. After the bubble is completely deformed, the pressure at the wall near the bubble increases due to the surface tension.

Fig. 10 shows the transient behavior of the relative viscosity for shearing a two-dimensional bubble. The relative viscosity was calculated during the simulation from the wall shear stress of the upper plate, which was divided by applied shear rate. For $\phi = 0.15$ and $Ca = 10$, the relative viscosity is about 0.80 initially and decreases with time. It means that less viscous dissipation occurs in the suspending fluid because the region where the flow changes its direction decreases as the bubble is deformed. For other cases, the relative viscosity increases a small amount with time and reaches a constant value. The reason is that the restoring force from the deformed bubble to its original shape keeps bubble from deformation so that the effects of the viscous dissipation and the surface tension on the viscosity become constant.

As we already mentioned in experimental results, the relative viscosity decreases more rapidly as the volume fraction increases in high capillary numbers. Fig. 11 shows the relative viscosities with respect to the capillary number. The simulation results are compared with the results from general equation determined based on experimental data and the Frankel and Acrivos equation. For the high capillary number and $\phi = 0.15$, the relative viscosity predicted by the numerical simulation is about 0.80, but Frankel and Acrivos equation yields about 0.77. The numerical simulation is based on a two-dimensional approach where the bubble is considered as a long circular cylinder. The interactions between the bubble and the plates exist in our simulation. Furthermore polydispersity of the bubbles and the interactions between bubbles are not considered numeri-
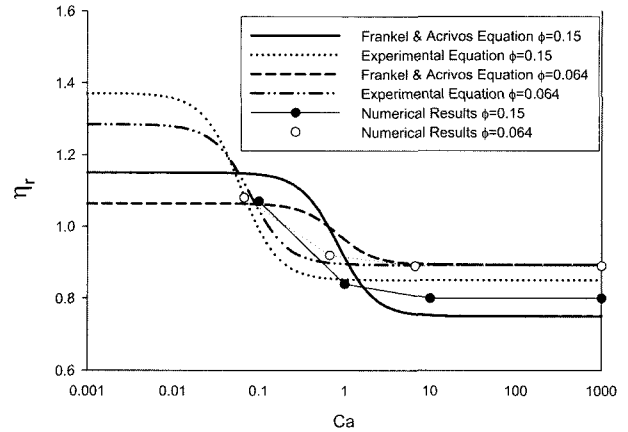
cally. Therefore numerical results cannot be compared with experimental results directly. Despite of these limitations, simulation results agree well with the general constitutive equation for high capillary numbers.

5. Conclusions

The viscosity of a polyol foam was measured in the case of low capillary numbers and various bubble volume fractions. Dilute bubble suspension in polyol shows shear thinning behavior. At low capillary number, increasing bubble volume fraction leads to an increase in viscosity, whereas at relatively high capillary number, viscosity decreases as bubble volume fraction increases. The general constitutive equation based on Frankel and Acrivos equation was derived as a function of bubble volume fraction and capillary number. Two dimensional numerical simulation was developed and carried out for high capillary number of unsteady region. Although numerical simulation has some restrictions, the numerical results are in good agreement with the experimental data. Three dimensional numerical simulation that can consider interactions between bubbles will be developed in the future work.

Acknowledgements

References

Brackbill, J.U., D.B. Kothe and C. Zemach, 1992, A continuum method for modeling surface tension, *Journal of Computational Physics* 100, 335.

Cho, W.J., H. Park and J.R. Youn, 1994, Ultrasonic bubble nucleation in reaction injection moulding of polyurethane, *Journal of Engineering Manufacture, Proc. Instn. Mech. Engrs. Part B* **208**, 121.

Cristini, V., J. Blawzdziewicz and M. Loewenberg, 1998, Drop breakup in three-dimensional viscous flows, *Physics of Fluids* **10**(8), 1781.

Frankel, N.A. and A. Acrivos, 1970, The constitutive equation for a dilute emulsion, *Journal of Fluid Mechanics* **44**, 65.

Kim, C. and J.R. Youn, 2000, Environmentally friendly processing of polyurethane foam for thermal insulation, *Polymer-Plastics Technology and Engineering* **39**(1), 163.

Koo, M.S., K. Chung and J.R. Youn, 2001, Reaction injection molding of polyurethane foam for improved thermal insulation, *Polymer Engineering and Science* **41**(7), 1177.

Lee, W.H., S.W. Lee, T.J. Kang, K. Chung and J.R. Youn, 2002, Processing of polyurethane/polystyrene hybrid foam and numerical simulation, *Fibers and Polymers* **3**(4), 159.

Leonard B.P., 1991, The ULTIMATE conservative difference scheme applied to unsteady one-dimensional advection, *Computer Methods in Applied Mechanics and Engineering* **88**, 17.

Llewellin, E.W., H.M. Mader and S.D.R. Wilson, 2002, The Rheology of a Bubbly Liquid, *Proceedings of the Royal Society of London. Series A* **458**, 987.

Loewenberg, M. and E.J. Hinch, 1996, Numerical simulation of a concentrated emulsion in shear flow, *Journal of Fluid Mechanics* **321**, 395.

Mackenzie, J.K., 1950, Elastic constants of a solid containing spherical holes, *Proceedings of the Royal Society of London. Series B* **63**, 2.

Macosko, C.V., 1994, Rheology: Principles, Measurements, and Applications, Willy, New York, 425.

Park, H. and J.R. Youn, 1992, Processing of cellular polyurethane by ultrasonic excitation, *Journal of Engineering for Industry,* *ASME Transactions* **114**(3), 323.

Park, H. and J.R. Youn, 1995, Processing of polyurethane microcellular foam by the reaction injection molding, *Polymer Engineering and Science* **35**(23), 1899.

Patankar, S.V., 1980, Numerical heat transfer and fluid flow, McGraw-Hill, New York.

Renardy, Y.Y. and V. Cristini, 2001, Effect of inertia on drop breakup under shear, *Physics of Fluids* **13**(1), 7.

Renardy, Y.Y., M. Renardy and V. Cristini, 2002, A new volume-of-fluid formulation for surfactants and simulations of drop deformation under shear at a low viscosity ratio, *European Journal of Mechanics B/Fluids* **21**, 49.

Rust, A.C. and M. Manga, 2002, Effects of bubble deformation on the viscosity of dilute suspensions, *Journal of Non-Newtonian Fluid Mechanics* **104**, 53.

Seo, D., J.R. Youn and C.L. Tucker III, 2003, Numerical simulation of mold filling in foam reaction injection molding, *International Journal for Numerical Methods in Fluids* **42**, 1105.

Taylor, G.I., 1932, Viscosity of a fluid containing small drops of another fluid, *Proceedings of the Royal Society of London. Series A* **138**, 41.

Tucker C.L. and P. Moldenaers, 2002, Microstructural Evolution in Polymer Blends, *Annual Reviews of Fluid Mechanics* **34**, 177.

Ubbink, O. and R.I. Issa, 1999, A Method for Capturing Sharp Fluid Interfaces on Arbitrary Meshes, *Journal of Computational Physics* **153**, 26.

Yan J. and F. Thiele, 1998, Performance and Accuracy of a Modified Full Multigrid Algorithm for Fluid Flow and Heat Transfer, *Numerical Heat Transfer, Part B* **34**, 323.

Youn, J.R. and H. Park, 1999, Bubble growth in reaction injection molded part foamed by ultrasonic excitation, *Polymer Engineering and Science* **39**(3), 457.